JOURNAL OF GUIDANCE, CONTROL, AND DYNAMICS
Vol. 15, No. 3, May-June 1992

Integrated Control of Thermally Distorted Large Space Antennas

Robert H. Tolson*
NASA Langley Research Center, Hampton, Virginia 23665
and
Jen-Kuang Huang†
Old Dominion University, Norfolk, Virginia 23529

The objective of this paper is to develop a control system design method that 1) recognizes the time dependence of the thermal distortion due to orbital motion and 2) controls variables that are directly related to far-field performance for Earth-pointing space antennas. The first objective is accomplished by expanding the distortion into principal components that are orthogonal in space and time. Actuator strokes become a linear combination of the time-dependent components. The spatial components provide a natural space in which to determine the optimal actuator locations and act as basis vectors for extrapolating sensor measurements to the entire antenna surface. The approach for the second objective is to expand the far zone electric field in a Zernike-Bessel series. The coefficients of this series provide a reliable measure of far-field performance and a natural cost function for designing the control system. The method accommodates tapered feeds and arbitrary polarizations. Simulations are performed for a geosynchronous radiometer to determine the effectiveness of the control system under variations in solar geometry, structure materials, and thermal properties.

Nomenclature

A_{nm}, B_{nm}, C_{nm} = amplitudes of Zernike polynomial expansion
a = antenna radius, m
E_i = electric field incident on the antenna surface, V/m
e_* = unit vector in direction $*$
F = antenna focal length, m
G = antenna feed gain function
J_1 = Zernike-Bessel cost
J_2 = Zernike-Bessel average cost over an orbit
J_S = antenna surface currents, A/m
k = wave number, $2\pi/\lambda$, m^{-1}
L = number of principal components used to calculate ϵ_α
M = number of actuators
N = number of points used to discretize the far-field integral
N_{nm} = Zernike polynomial normalization factor
P_t = total power radiated by the feed, W
R, Θ, Φ = coordinates of far-field point
R_{nm} = Zernike radial polynomial
S = number of sensors
s_α = stroke of αth actuator, m
$\alpha_{nm}, \beta_{nm}, \gamma_{nm}$ = phases of Zernike polynomial expansion
γ = argument of Bessel series, $ka \sin\Theta$
δ_i^j = Kronecker delta
ϵ, μ, η = free space permittivity, permeability, and impedance
$\epsilon_\alpha, \epsilon_{\alpha\beta}$ = rod effectiveness and correlation ratios
λ = electromagnetic wavelength, m
ρ, θ, φ = coordinates of antenna surface point
τ = nondimensional radius, $(\rho/a)\sin\theta = (2F/a)\tan(\theta/2)$
Ψ = wave aberration function, m
ω = electromagnetic angular frequency, s^{-1}

Received April 4, 1991; presented as Paper 91-0965 at the AIAA/ASME/ASCE/AHS/ASC 32nd Structures, Structural Dynamics, and Materials Conference, Baltimore, MD, April 8-10 1991; revision received July 22, 1991; accepted for publication July 23, 1991.

*Senior Research Engineer, Mail Stop 269. Associate Member AIAA.
†Associate Professor, Department of Mechanical Engineering and Mechanics. Member AIAA.

I. Introduction

DISTORTION of large space antennas can be due to a number of causes, many of which must be corrected in orbit. Methods for correcting surface distortions due to manufacturing and fabrication tolerances[1,2] and structural vibration[3] have been reported. Controlling thermally distorted space antennas has received limited attention even though controlling thermal distortions of Earth-based optical telescopes is an active research area.[4] Methods have been developed for single orbital heating conditions (i.e., static shape control) based on minimizing the rms surface deviation, and optimal actuator locations have also been determined for the same case.[5] No studies address the temporal variation of the distortion field and the subsequent effect on the optimal locations. In addition, surface rms may not be the most appropriate objective function since space antenna feeds may be highly tapered and surface errors in highly illuminated areas will degrade performance more than the same error in other areas. This paper presents a method for designing a system to control the effects of thermal distortion on antenna performance due to the temperature variations in orbit. The method recognizes the time dependence of the distortion in determining actuator locations and also controls variables that are directly related to antenna performance.

II. Antenna Performance

The performance of a space antenna is characterized by its far zone electric field pattern.[6] Specific performance parameters include gain, cross polarization, side lobe levels, and beam efficiency. These parameters are related to antenna surface

shape by nonlinear functions and consequently are not desirable linear control system objectives. One approach to controlling such parameters for the case of manufacturing errors was solved as a nonlinear programming problem.[1] Though computationally intensive, the study showed the benefits of directly controlling electromagnetic parameters in lieu of the traditional rms surface deviation.

For distortions that are small relative to the wavelength, it is possible to expand the far zone electric field in a Zernike-Bessel series,[7] and in so doing a quadratic cost function naturally appears. A summary of this derivation is presented here. The coordinate system is shown in Fig. 1, where the origin is at the parabolic focus (feed).

The electric field incident on the antenna from the feed is[6]

$$\boldsymbol{E}_i(\rho,\theta,\varphi) = \left\{\sqrt{\mu/\epsilon}\,\frac{P_t}{2\pi}\,G(\theta,\varphi)\right\}^{1/2}\frac{e^{-jk\rho}}{\rho}\,\boldsymbol{e}_i$$

Such an incident electric field induces surface currents of[6]

$$\boldsymbol{J}_S = 2\sqrt{\epsilon/\mu}\,\left[\boldsymbol{e}_n \times (\boldsymbol{e}_\rho \times \boldsymbol{E}_i)\right]$$

where $\boldsymbol{e}_n$ is normal to the surface. These surface currents produce a far zone electric field given by an integral over the surface of the antenna[6]

$$\boldsymbol{E} = -\frac{j\omega\mu e^{-jkR}}{4\pi R}\iint_S \boldsymbol{J}_S \exp\left[jk\rho(\boldsymbol{e}_\rho\cdot\boldsymbol{e}_R)\right]\,dS$$

Substituting for $\boldsymbol{J}_S$ and $\boldsymbol{E}_i$, letting $\boldsymbol{u} = \boldsymbol{e}_n \times (\boldsymbol{e}_\rho \times \boldsymbol{e}_i)$ and collecting terms outside the integral into C_1 gives[7]

$$\boldsymbol{E} = C_1\iint_S \boldsymbol{u}\sqrt{G}\,\frac{\exp\left[-jk\rho(1-\boldsymbol{e}_\rho\cdot\boldsymbol{e}_R)\right]}{\rho}\,dS \qquad (1)$$

This is the fundamental integral of physical optics, and numerical evaluation methods include two-dimensional quadrature and infinite series expansions.[8,9] The interest here, however, is in obtaining an analytic cost function that will measure the contribution of the distortion of the antenna to the far-field pattern. To this end, two assumptions are made: first, only the effects of antenna surface distortion on the phase of the reflected rays will be considered, and second, angular deviations from the central beam $\Theta = \pi$ and the ratio of wavelength to focal length (λ/F) are both considered small to first order. Neglecting second-order terms and after considerable algebra, Eq. (1) becomes[7]

$$\boldsymbol{E} = C\int_0^{2\pi}\int_0^1 \boldsymbol{u}\sqrt{G}\left[1 - 2\sin^2\frac{k\Psi}{2} - j\sin k\Psi\right]$$
$$\times \cos\theta/2\exp\left[jka\tau\sin\Theta\right]\cos(\Phi-\varphi)\tau\,d\tau\,d\varphi \qquad (2)$$

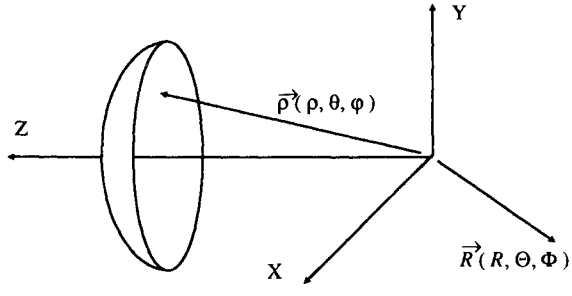

Fig. 1 Coordinate system.

where

$$C = -\frac{j\omega\mu a^2\left[\exp -jk(R+2F)\right]}{2\pi RF\eta}\left\{\sqrt{\mu/\epsilon}\,\frac{P_t}{2\pi}\right\}^{1/2}$$

In Eq. (2), the surface distortion is represented by Ψ, the wave aberration function[10] in the aperture plane (i.e., the plane $z = 0$). For a parabolic reflector, the distance traveled by a ray from the focus to the aperture plane is $2F$; Ψ is the distance traveled by a ray from the focus to the aperture plane of the distorted antenna minus $2F$. Under the earlier assumptions, $\Psi = (1+\cos\theta)\delta z$ and is linear in the surface distortion.[7] For shallow reflectors, Ψ is twice the z component of distortion.

The final step is to reduce Eq. (2) to an infinite series by using a Zernike polynomial expansion.[10] The Zernike polynomials, $Z_{nm}(\tau,\varphi,\varphi_{nm}) = R_{nm}(\tau)\cos m(\varphi-\varphi_{nm})$, are orthogonal on the unit circle, complete with respect to the ring of polynomials in x and y, and defined for n from 0 to ∞ and for m from 0 to n with n-m even. The Zernike radial polynomials in the normalized radius are $R_{nm}(\tau)$. Assuming that $\boldsymbol{U}$, $\boldsymbol{V}$, and $\boldsymbol{W}$, as defined later, admit to Taylor series expansions, then $\boldsymbol{A}_{nm}$, $\boldsymbol{B}_{nm}$, $\boldsymbol{C}_{nm}$, α_{nm}, β_{nm}, and γ_{nm} exist such that

$$\boldsymbol{U}(\theta,\varphi) \equiv \boldsymbol{u}\sqrt{G}\,\cos\theta/2 = \sum_{n,m}\boldsymbol{A}_{nm}Z_{nm}(\tau,\varphi,\alpha_{nm}) \qquad (3)$$

$$\boldsymbol{V}(\theta,\varphi) \equiv 2\boldsymbol{U}(\theta,\varphi)\sin^2\frac{k\Psi}{2} = \sum_{n,m}\boldsymbol{B}_{nm}Z_{nm}(\tau,\varphi,\beta_{nm}) \qquad (4)$$

$$\boldsymbol{W}(\theta,\varphi) \equiv \boldsymbol{U}(\theta,\varphi)\sin k\Psi = \sum_{n,m}\boldsymbol{C}_{nm}Z_{nm}(\tau,\varphi,\gamma_{nm}) \qquad (5)$$

Note that τ and θ are equivalent variables. Introduce these expansions into Eq. (2) along with the well-used expansion of the exponential in Bessel functions

$$\exp\left[jka\tau\sin\Theta\right]\cos(\Phi-\varphi) = J_0(ka\tau\sin\Theta)$$
$$+ 2\sum_{p=1}^{\infty} j^p J_p(ka\tau\sin\Theta)\cos p(\Phi-\varphi)$$

and integrate with respect to φ term by term using the usual Fourier orthogonality conditions. The remaining integral over τ is performed by using the relation[10]

$$\int_0^1 R_{nm}(\tau)J_m(\gamma\tau)\tau\,d\tau = (-1)^{(n-m)/(2)}\frac{J_{n+1}(\gamma)}{\gamma}$$

Equation (2) is thereby reduced to the infinite series

$$\boldsymbol{E} = 2\pi C\sum_n \frac{J_{n+1}(\gamma)}{\gamma}\sum_m j^m(1+\delta_m^0)(-1)^{(n-m)/(2)}$$
$$\times\left\{\boldsymbol{A}_{nm}\cos m(\Phi-\alpha_{nm}) - \boldsymbol{B}_{nm}\cos m(\Phi-\beta_{nm})\right.$$
$$\left. - j\boldsymbol{C}_{nm}\cos m(\Phi-\gamma_{nm})\right\} \qquad (6)$$

The coefficients $\boldsymbol{A}_{nm}$ determine the far zone electric field of the undistorted reflector and the coefficients $\boldsymbol{B}_{nm}$ and $\boldsymbol{C}_{nm}$ determine the contribution to the field due to the distortions of the reflector. $\boldsymbol{A}_{00}$ determines the undistorted field along the centerline ($\Theta = \pi$) and will be used later to normalize results presented in decibels. Explicit expressions for $\boldsymbol{A}_{nm}$, $\boldsymbol{B}_{nm}$, and $\boldsymbol{C}_{nm}$ and the corresponding phases can be obtained using inverse integral relations.[10] For example,

$$\boldsymbol{C}_{nm}e^{j\gamma_{nm}} = \frac{2}{\pi N_{nm}}\int_0^{2\pi}\int_0^1 W(\tau,\varphi)R_{nm}(\tau)e^{jm\varphi}\tau\,d\tau\,d\varphi \qquad (7)$$

where $N_{nm} = (1+\delta_m^0)/(n+1)$ normalizes the integral of each squared Zernike polynomial over the unit circle to unity.[11]

III. Cost Functions

The control system must restore the thermally distorted far-field pattern to an acceptable level of agreement with the undisturbed pattern. The $\boldsymbol{B}_{nm}$ and the $\boldsymbol{C}_{nm}$ determine the contribution of the surface distortion to the far-field pattern. A natural objective would be to minimize their contribution in some quadratic manner. One such measure is

$$J_1 \equiv \sum_{n,m} N_{nm}\boldsymbol{C}_{nm} \cdot \boldsymbol{C}_{nm} = \frac{2}{\pi}\iint_S \boldsymbol{W} \cdot \boldsymbol{W}\, \mathrm{d}S \tag{8}$$

where the equality follows from Parseval's theorem. For the level of distortion acceptable for radiometers, $|\Psi| < (\lambda/4) = (\pi/2k)$, so $2\sin^2(k\Psi/2) < |\sin k\Psi|$ and, consequently,

$$\iint_S \boldsymbol{V} \cdot \boldsymbol{V}\, \mathrm{d}S < \iint_S \boldsymbol{W} \cdot \boldsymbol{W}\, \mathrm{d}S$$

Thus, by Parseval's theorem,

$$\sum_{n,m} N_{nm}\boldsymbol{B}_{nm} \cdot \boldsymbol{B}_{nm} < \sum_{n,m} N_{nm}\boldsymbol{C}_{nm} \cdot \boldsymbol{C}_{nm}$$

and controlling the latter sum assures control of the former. To complete the process of linearizing the problem, it is assumed that $k\Psi$ is sufficiently small that the small angle approximation is valid. The $\boldsymbol{C}_{nm}$ are now linearly related to reflector displacements and the cost function J_1 is therefore quadratic in the displacements. A quadratic penalty in actuator stroke could be appended to J_1 for a slight additional complexity in the algebra to, for example, limit structural stress. The problem has thus been put into a traditional control problem format. Noted that J_1 is approximately the surface deviation rms for linearly polarized antennas with uniform aperture power. J_1 will be called the "Zernike-Bessel" cost because it was from Eq. (6) that the contribution of each term in Eq. (2) could be related to the far-field power. However, in what follows, J_1 will be calculated using the integral part of Eq. (8) rather than Eq. (7).

Still no consideration has been given to the fact that the antenna distortions and therefore the $\boldsymbol{C}_{nm}$ are time dependent. To include the temperal variations of the distortions, the "Zernike-Bessel average cost" is defined by

$$J_2 = \frac{1}{P}\int_0^P J_1(t)\, \mathrm{d}t = \frac{1}{P}\int_0^P \sum_{n,m} N_{nm}\boldsymbol{C}_{nm} \cdot \boldsymbol{C}_{nm}\, \mathrm{d}t \tag{9}$$

Recall that for the undistorted antenna $\boldsymbol{E}(\pi,0) = \pi C\boldsymbol{A}_{00}$. Possible goals for the control system might be to control $J_1/\boldsymbol{A}_{00}\cdot\boldsymbol{A}_{00}$ or $J_2/\boldsymbol{A}_{00}\cdot\boldsymbol{A}_{00}$ to be less than -20 dB, since this would imply that the terms in Eq. (6) representing the antenna distortion are contributing no more than 1% of the power at the center of the beam. In the following, it is assumed that the control system articulates only the antenna surface. An alternate approach is to assume that the feed location can also be changed to control piston[11] (C_{00}) and tilt (C_{11}). This would be equivalent to locating the feed at the focus of the "best fit parabola" and evaluating Eqs. (3–5) based on that parabola.

IV. Principal Component Decomposition

The temporal variations can be included in the development of optimal actuator locations by performing a principal component decomposition of the linearized version of $\boldsymbol{W}$ given by Eq. (5). The salient feature of principal component analysis, as used here, is the ability to decompose a time-dependent spatial vector field into components that are both spatially and temporally orthogonal.

For a sufficiently large number of points (τ_i,φ_i), $i = 1,\ldots,N$ suitably distributed over the aperture $0 \le \tau \le 1$, $0 \le \varphi \le 2\pi$, the quadrature for $\boldsymbol{C}_{nm}\exp j\gamma_{nm}(t)$ of Eq. (7) can be approximated by

$$\frac{2}{\pi N_{nm}}\sum_{i=1}^{N} \boldsymbol{W}(\tau_i,\varphi_i,t)R_{nm}(\tau_i)e^{jm\varphi_i}\Delta S \tag{10}$$

where $\Delta S = \tau_i\, \mathrm{d}\tau_i\, \mathrm{d}\varphi_i = \pi/N$ is independent of i. With such a set of points, form the $N \times 3$ matrix

$$\boldsymbol{G}(t) = \left[\boldsymbol{W}(\tau_1,\varphi_1,t), \boldsymbol{W}(\tau_2,\varphi_2,t), \ldots, \boldsymbol{W}(\tau_N,\varphi_N,t)\right]^T \tag{11}$$

The discussion of the principal components follows the development of Moore.[12] Form the Grammian:

$$\boldsymbol{H} = \frac{1}{P}\int_0^P \boldsymbol{G}(t)\boldsymbol{G}^T(t)\, \mathrm{d}t \tag{12}$$

where $\boldsymbol{H}$ is a symmetric, positive, semidefinite matrix with nonnegative "principal eigenvalues" $\sigma_1^2 \ge \sigma_2^2 \ldots \ge \sigma_N^2 \ge 0$ and real, orthogonal, unit "principal eigenvectors" $\boldsymbol{e}_1,\boldsymbol{e}_2,\ldots,\boldsymbol{e}_N$. $\boldsymbol{G}$ can be expanded in terms of the eigenvectors as

$$\boldsymbol{G} = \sum_{i=1}^{N} \boldsymbol{e}_i\boldsymbol{g}_i^T(t) = \boldsymbol{E}\boldsymbol{G}_e \tag{13}$$

where the eigenvectors are columns of $\boldsymbol{E}$ and the "principal component amplitudes"

$$\boldsymbol{g}_i(t) = \boldsymbol{G}^T(t)\boldsymbol{e}_i \tag{14}$$

are rows in the $N \times 3$ matrix $\boldsymbol{G}_e$. Equation (13) is therefore an expansion of $\boldsymbol{G}$ in a set of time-dependent, spatially orthogonal "principal components" $\boldsymbol{e}_i\boldsymbol{g}_i^T(t)$ that are also temporally orthogonal since[12]

$$\frac{1}{P}\int_0^P \boldsymbol{g}_p^T(t)\boldsymbol{g}_q(t)\, \mathrm{d}t = \sigma_q^2\delta_p^q \tag{15}$$

For later reference, note that from Eqs. (13) and (14)

$$\|\boldsymbol{G}\|^2 = \|\boldsymbol{G}_e\|^2 = \sum_{i=1}^{N} \boldsymbol{g}_i^T\boldsymbol{g}_i \tag{16}$$

The Zernike-Bessel costs of Eqs. (8) and (9) can now be related to the principal component decomposition. First

$$\|\boldsymbol{G}\|^2 = \mathrm{tr}\,\boldsymbol{G}\boldsymbol{G}^T = \sum_{i=1}^{N} \|\boldsymbol{W}(\tau_i,\varphi_i,t)\|^2 \approx \frac{N}{\pi}\iint_S \|\boldsymbol{W}(\tau,\varphi,t)\|^2\, \mathrm{d}S$$

But

$$\iint \|\boldsymbol{W}\|^2\, \mathrm{d}S = \frac{\pi}{2}\sum_{n,m} N_{nm}\boldsymbol{C}_{nm} \cdot \boldsymbol{C}_{nm} = \frac{\pi}{2}J_1$$

Thus,

$$J_1 \approx \frac{2}{N}\|\boldsymbol{G}\|^2 = \frac{2}{N}\sum_{i=1}^{N} \boldsymbol{g}_i^T\boldsymbol{g}_i \tag{17}$$

Also

$$\sum_{n=1}^{N} \sigma_i^2 = \mathrm{tr}\,\boldsymbol{H} = \frac{1}{P}\int_0^P \mathrm{tr}\,\boldsymbol{G}\boldsymbol{G}^T\, \mathrm{d}t \approx \frac{N}{2P}\int_0^P J_1\, \mathrm{d}t = \frac{N}{2}J_2$$

So

$$J_2 = \frac{1}{P}\int_0^P J_1(t)\, \mathrm{d}t \approx \frac{2}{N}\sum_{i=1}^{N} \sigma_i^2 \tag{18}$$

One of the rationales for using the principal component decomposition is the expectation that the eigenvalues decrease rapidly so that J_2 is dominated by a small number of eigenval-

ues. In this case, the control system will be required to control only the far-field distortion due to the eigenfunctions corresponding to the reduced set.

V. Control System Design

The system under discussion is similar to a static shape control system, and consequently the issues are how many sensors and actuators should be used, where should they be located, how should the actuators be controlled, and how should the sensor data be processed. In this section, the actuator control laws will be derived assuming perfect knowledge of the distortions, a method will be given for determining optimal actuator locations using the Zernike-Bessel average cost, and a method for processing sensor data to directly estimate the contribution of the distorted shape to the far field will be presented.

Control with Actuators Fixed

First consider a system when the actuator locations are known. Let there be M actuators at preselected sites. For the αth actuator $\alpha = 1, \ldots, M$, a unit stroke will produce a reflector surface displacement field that can be converted to a phase function $\Psi_\alpha(\tau,\varphi)$ and then by Eq. (5) to a $W_\alpha(\tau,\varphi)$ field. As was done earlier for the thermal distortion field, the control field can be discretized to form a $N \times 3$ matrix for each of the M actuators

$$G_\alpha = \left[W_\alpha(\tau_1,\varphi_1),\ W_\alpha(\tau_2,\varphi_2),\ W_\alpha(\tau_N,\varphi_N),\right]^T \tag{19}$$

Let s_α represent the stroke of the αth actuator. The goal is to select a set of s_α so that the difference δG between the thermal distortion and the actuator-induced distortions has minimum Euclidean norm, that is, minimize

$$\|\delta G\| \equiv \left\| G - \sum_{\alpha=1}^{M} s_\alpha G_\alpha \right\| = \left\| G_e - \sum_{\alpha=1}^{M} s_\alpha F_{e_\alpha} \right\|^2 \tag{20}$$

where G_e is given by Eq. (13),

$$G_\alpha = \sum_{i=1}^{N} e_i f_{\alpha_i}^T = E F_{e_\alpha}, \qquad f_{\alpha_i} = G_\alpha^T e_i$$

is 3×1 and $F_{e_\alpha} = E^T G_\alpha$ is $N \times 3$.

This is a classical least square problem of finding the M values of s_α that minimize the sum of squares of the elements in the δG matrix. In terms of G and G_α, the usual solution approach gives

$$\begin{bmatrix} G_{1*}+G_1, & \cdots & G_{M*}+G_1 \\ G_{1*}+G_2, & \cdots & G_{M*}+G_2 \\ \vdots & \vdots\vdots & \vdots \\ G_{1*}+G_M, & \cdots & G_{M*}+G_M \end{bmatrix} \begin{vmatrix} s_1 \\ s_2 \\ \vdots \\ s_M \end{vmatrix} = \begin{vmatrix} G_*+G_1 \\ G_*+G_2 \\ \vdots \\ G_*+G_M \end{vmatrix} \tag{21}$$

where $A_* + B$ is a shorthand notation for the sum of the element-by-element products of A and B, e.g., $\|A\|^2 = (A_* + A)$. The solution gives $\hat{s}$, the vector of optimal actuator strokes that minimizes the Zernike-Bessel cost at any time.

In terms of G_e and F_{e_α}, Eq. (20) relates the optimal strokes to the principal component amplitudes. From this form, it is seen that the solution will give the s_α as linear combinations of the components of G_e, which are the time-dependent amplitudes of the principal components. Consequently, the optimal control for each actuator will be a linear combination of the principal component amplitudes. Actuator bandwidth can thus be determined by Fourier analysis of G_e.

Optimal Actuator Locations

In previous papers,[5] optimal actuator locations have been determined based on the single location in orbit that produced the worst thermal distortion. The performance of such a set was not evaluated at other locations in orbit. In this paper, the approach is to select the optimal locations based on the average performance over the orbital period. The relative advantages of these two approaches will be case dependent, and both approaches should probably be tested before locations are finalized. Consequently, for a fixed number of identical actuators M, the optimal actuator configuration will be defined as the one that minimizes J_2. To address this optimal location problem, it is convenient to put Eq. (20) into a standard vector least square format. Form the $3N$ vector y, the $3N \times M$ matrix F, and the M vector s:

$$y = \begin{vmatrix} g_1 \\ g_2 \\ \vdots \\ g_N \end{vmatrix}, \quad F = \begin{bmatrix} f_{1_1}, & \cdots & f_{M_1} \\ f_{1_2}, & \cdots & f_{M_2} \\ \vdots & \vdots\vdots & \vdots \\ f_{1_N}, & \cdots & f_{M_N} \end{bmatrix}, \quad s = \begin{vmatrix} s_1 \\ s_2 \\ \vdots \\ s_M \end{vmatrix} \tag{22}$$

In this notation, $\|\delta G\| = \|y - Fs\|$, with the least square solution $\hat{s}$ given by $\hat{s} = [F^T F]^{-1} F^T y$. The minimum norm is $\|\delta \hat{G}\|^2 \equiv \|y - F\hat{s}\|^2 = y^T P y$, where P is the idempotent projection associated with the least square estimator,

$$P = I - F(F^T F)^{-1} F^T \tag{23}$$

So

$$J_1 = \frac{2}{N} \|\delta \hat{G}\|^2 = \frac{2}{N}\, y^T P y \tag{24}$$

In the case of a linearly polarized aperture electric field, both G and G_α are vectors, and an explicit relation between the minimum norm and the eigenvalues can be obtained. When $y(i) = g_i$, then

$$\|\delta \hat{G}\|^2 = \sum_{i=1}^{N} \sum_{j=1}^{N} g_i P(i,j) g_j$$

Recalling Eq. (18), form the integral over the period to get

$$J_2 = \sum_{i=1}^{N} \sum_{j=1}^{N} \frac{2}{NP} \int_0^P g_i P(i,j) g_j \, dt = \sum_{i=1}^{N} \sigma_i^2 P(i,i) \tag{25}$$

which is the trace of the projector weighted by the eigenvalues.

Returning to the general case, only y is time dependent in Eq. (24) so perform the quadrature

$$Y(i,j) \equiv \frac{1}{P} \int_0^P y(i) y(j) \, dt$$

The Zernike-Bessel average cost can then be written as

$$J_2 = \frac{2}{N} \sum_{i=1}^{3N} \sum_{j=1}^{3N} Y(i,j) P(i,j) \tag{26}$$

It can be shown[7] using Cauchy's inequality and Eq. (15) that $[Y(i,j)]^2 \le \sigma_{k_i}^2 \sigma_{k_j}^2$, where k_i is the principal component corresponding to y_i. Thus, if the eigenvalues decrease rapidly, a partial sum will be adequate to evaluate Eq. (26) in the search for optimal locations.

Minimizing J_2 is a discrete optimization problem with no known algorithm to obtain the optimum except exhaustive search.[13] Approximate solutions to similar problems include identifying the least effective occupied location and the most effective unoccupied location and interchanging until there is no improvement in the objective.[5] For Eq. (26) it is possible to develop a method that optimally adds an additional actuator. Let P in Eq. (23) and F in Eq. (22) correspond to some actuator configuration and P_+ and F_+ be the same configuration with one additional actuator. The task is to find an expression for

P_+ that does not require a new matrix inverse. First write $F_+ = |F, f|$, where f is the additional column to be appended to F for the additional actuator. The required expression can be developed from the well-known relation for the inverse of a partitioned symmetric matrix to give

$$(F_+^T F_+)^{-1} = \begin{vmatrix} F^T F, & F^T f \\ f^T F, & f^T f \end{vmatrix}^{-1}$$

$$= \begin{vmatrix} (F^T F)^{-1} + \dfrac{(F^T F)^{-1} F^T f f^T F (F^T F)^{-1}}{f^T P f}, & \dfrac{-(F^T F)^{-1} F^T f}{f^T P f} \\ \dfrac{-f^T F (F^T F)^{-1}}{f^T P f}, & \dfrac{1}{f^T P f} \end{vmatrix}$$

Using Eq. (23) for both P and P_+ gives

$$P_+ = P + \frac{P f f^T P^T}{f^T P f} \tag{27}$$

Given any configuration of actuators, Eq. (27) provides the basis for identifying the most effective actuator for augmentation of the configuration. The final result is, of course, a suboptimal solution.

For large structures there may be a great number of potential sites, and it is convenient to restrict the total set to a smaller subset of the "most effective" sites before beginning any search technique. An approximate means of doing this is demonstrated for the linearly polarized case. Suppose that the sensitivity matrix for each of the actuators G_α, a vector for this case, is a linear combination of only the eigenvectors corresponding to the L largest eigenvalues. Then $f_{\alpha_i} = 0$ for $i = L+1, L+2, \ldots, N$, and so F_{e_α} has the form

$$F_{e_\alpha} = \begin{vmatrix} F_L \\ \mathbf{0} \end{vmatrix}$$

where F_L is an $L \times L$ matrix that is assumed to have full rank so that the s_α have a solution. In this case,

$$P = I - \begin{vmatrix} F_L (F_L^T F_L)^{-1} F_L^T, & \mathbf{0} \\ \mathbf{0}, & \mathbf{0} \end{vmatrix} = \begin{vmatrix} \mathbf{0} & \mathbf{0} \\ \mathbf{0} & I \end{vmatrix}$$

so that Eq. (25) becomes

$$J_2 = \frac{\pi}{N} \sum_{i=L+1}^{N} \sigma_i^2$$

The L largest eigenvalues are therefore excluded from the cost, and it can be shown[12] that this is the minimum cost for any L actuators. The result does not extend easily to the general polarization case but does suggest that a criteria for ordering potential actuators sites is the "effectiveness" ratio

$$\epsilon_\alpha \equiv \frac{\sum_{i=1}^{L} f_{\alpha_i}^T f_{\alpha_i}}{\sum_{i=1}^{N} f_{\alpha_i}^T f_{\alpha_i}} = \frac{\sum_{i=1}^{L} f_{\alpha_i}^T f_{\alpha_i}}{\|G_\alpha\|^2} = \frac{\|F_{\alpha_L}\|^2}{\|G_\alpha\|^2} \tag{28}$$

where $F_{\alpha_L} = G_\alpha^T E_L$ and E_L is the $N \times L$ matrix of the first L eigenvectors. Also,

$$\sum f_{\alpha_i}^T f_{\alpha_i} = \|F_{e_\alpha}\|^2 = \|G_\alpha\|^2$$

has been used in the denominator. The effectiveness is a relative measure of the extent to which the αth sensitivity matrix can be represented as a linear combination of the first L eigenvectors. If $\epsilon_\alpha = 1$, then the columns of G_α are vectors in the hyperplane determined by the first L eigenvectors, and the first L principal components can be influenced without "exciting" the remaining principal components. On the other hand, when $\epsilon_\alpha = 0$, the columns of G_α are orthogonal to the hyperplane and locating actuators at such sites cannot reduce the contribution of the first L eigenvalues to J_2.

Even though ϵ_α provides a means of ordering the possible actuator location sites, care must be exercised in the use of such an ordering. If two sites could produce the same G_α, they would have the same ϵ_α, but including both in the potential site list is clearly redundant. The goal is to pick actuator sites that are effective as measured by ϵ_α but are also "orthogonal." One measure of orthogonality, to be used later, is the rod "correlation factor" for two actuator sites α and β

$$\epsilon_{\alpha\beta} \equiv \frac{\sum_{i=1}^{L} f_{\alpha_i}^T f_{\beta_i}}{\|F_{\alpha_L}\| \, \|F_{\beta_L}\|} \tag{29}$$

Processing Sensor Data

Assume the availability of S sensors that measure the displacement of the reflecting surface from the nominal shape and M actuators. With $M \geq S$ properly located actuators, it is straightforward to eliminate the distortion at the S measurement locations, and with $M < S$ the error can be reduced in an rms sense. In either case, there is no physically meaningful way to calculate displacements at other locations on the surface, perhaps limiting the effectiveness of the measurements. To overcome this situation, the principal components, which represent the expected global deviation, are used to effectively extrapolate the measurements to the entire surface. First the measurements are converted into phase shift Ψ, then the phase shift field is expanded in principal components, and finally the amplitudes of the principal components of Eq. (15) are estimated from the measurements. The minimum number of sensors is thus the number of principal components that must be controlled to meet the performance goal. Once the principal component amplitudes have been estimated, an estimate $\hat{G}$ of G can be made using Eq. (13). Then the actuator strokes s_α will be selected, using Eq. (21), to minimize the norm of

$$\delta G = \hat{G} - \sum_{\alpha=1}^{M} s_\alpha G_\alpha$$

where $\hat{G}$ is an estimate of G obtained from the sensors.

Before formulating an estimator for G, note that the three columns of G are not independent, since they are just the three components of W in Eq. (11), which are related by the three components of u through Eq. (5). Thus if one component is known, the other two can be calculated. Conversely, there is only a need to estimate the amplitude corresponding to one column of the G matrix. For example, if the y component is selected, Eq. (13) reduces to $W_y = E g_y$. Since the chosen component is arbitrary, the subscript will be dropped in the following. Let P be the number of components of g to be estimated from S measurements. The observation equation is therefore

$$W_s = E_{sp} g_p \tag{30}$$

where W_s is the measured vector, g_p is the P vector to be estimated, and E_{sp} is an $S \times P$ matrix of the appropriate elements of E of Eq. (13). Assuming zero mean measurement errors for W_s, Eq. (30) becomes a classical estimation problem with minimum variance solution

$$\hat{g}_p = [E_{sp}^T \Gamma^{-1} E_{sp}]^{-1} E_{sp}^T \Gamma^{-1} W_s \tag{31}$$

where Γ is the covariance on the measurement vector $\hat{W}_s$, which is calculated from the covariance on the fundamental measurements of surface displacement.

From $\hat{g}_p$, the entire column W of G is obtained by

$$\hat{W} = E_p \hat{g}_p \tag{32}$$

where E_p are the appropriate columns of E. The other two columns of G can be calculated as mentioned earlier to give the final estimate $\hat{G}$.

The remaining problem is how many sensors to place on the surface and where to place them. Like the optimal actuator location problem, this is a discrete optimization problem and there are a number of discrete optimization approaches[13] that, for example, maximize the trace of the information matrix associated with Eq. (31).

VI. Validation Studies

In this section the previous developments will be tested using (Fig. 2) a 55-m tetrahedral truss, space radiometer.[1,5] Specific structural properties[14] have been slightly modified[7] to provide adequate buckling margin with the 1-mm strokes of the actuators. The antenna is assumed to be in a geosynchronous orbit (GEO) with the z axis of the antenna (Fig. 1) pointing directly away from the center of the Earth and the y axis normal to the orbit plane in the same direction as the orbital angular momentum vector. Temperature deviations for each structural rod were calculated using the time-dependent energy balance equation.[15] Temperature differences between individual rods at some positions in orbit are over 150 K. From these temperature calculations a linear structural analysis yields the displacements of the truss grid points. To calculate reflecting surface distortions from these grid point displacements, it is assumed that a reflecting knitted mesh is supported on the truss structure and that the triangle of mesh between structural nodes behaves like a rigid surface. The displacement of any point on the mesh is thus modeled as a linear combination of the displacements of the three truss nodes surrounding the point.

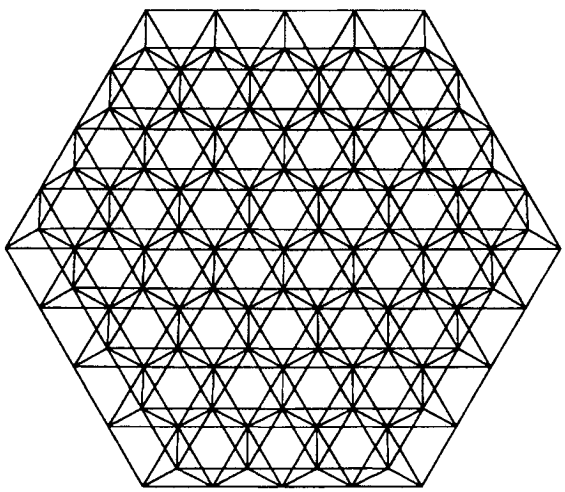

Fig. 2 55-m tetrehedral truss.

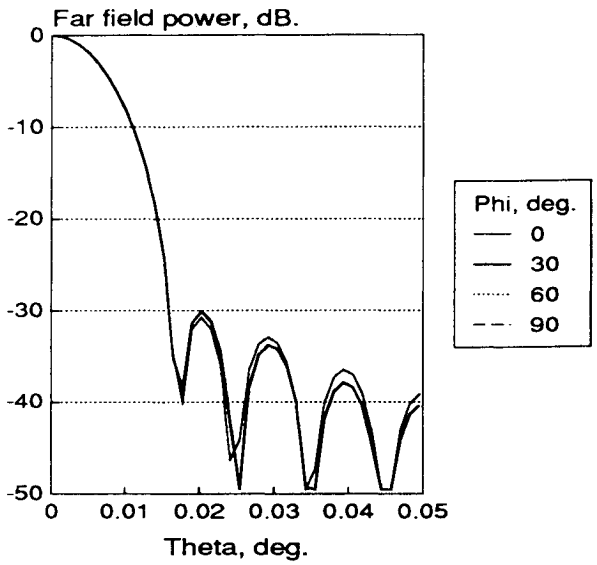

Fig. 3 Far-field pattern for 55-m parabolic reflector.

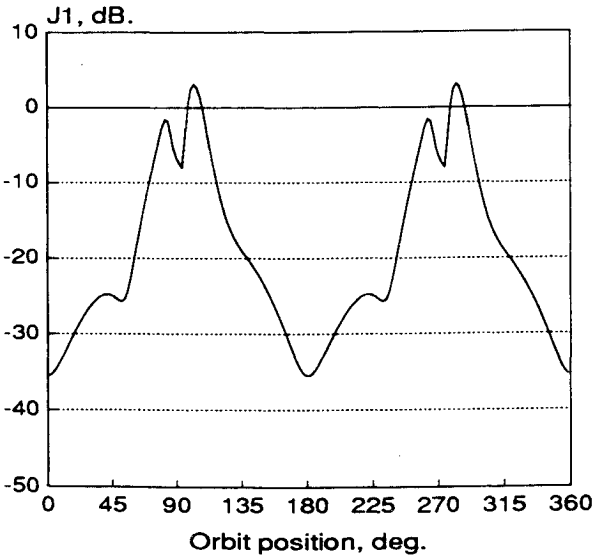

Fig. 4 Temporal variation of nominal orbit cost J_1.

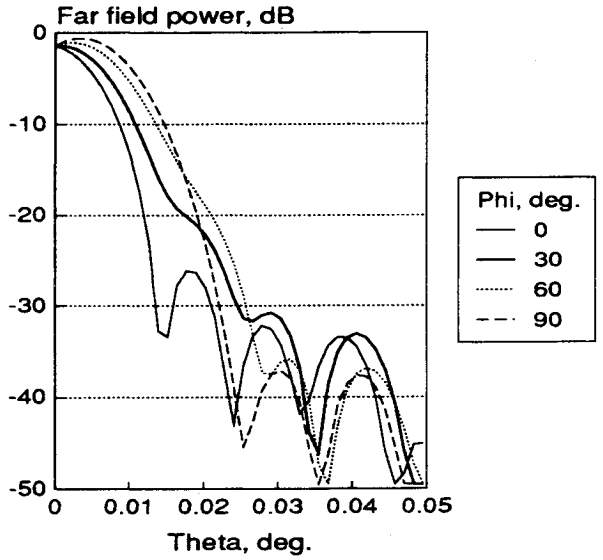

Fig. 5 Far-field pattern at maximum cost J_1.

The 55-m antenna has a focal length of 82.5 m. An operating frequency of 30 GHz is assumed along with a y-polarized feed so that u has the form given by[8]

$$u = \frac{\cos\theta/2}{\sqrt{1-\sin^2\varphi\,\sin^2\theta}}\left[-\sin 2\varphi\,\sin^2\theta/2\,\boldsymbol{e}_x + (1-2\sin^2\varphi\,\sin^2\theta/2)\boldsymbol{e}_y + \sin\varphi\,\cos\theta\,\sin\theta/2\,\boldsymbol{e}_z\right]$$

High-resolution radiometers will have highly tapered feeds to increase beam efficiency by suppressing the side lobes. A -30 dB level is used as the design value for the undistorted surface. The control system will not be able to maintain the -30 dB level, so the goal for the control system will be to maintain the side lobes below -28 dB. To meet the -30 dB design level, a cosine power law[8] is used for the feed gain function of Eq. (1):

$$G(\theta) = 126\cos^{62}\theta, \quad 0 \le \theta \le \frac{\pi}{2} \quad \text{and} \quad G(\theta) = 0 \ \text{otherwise}$$

Figure 3 shows four sections through the far-field pattern for a parabolic surface with this taper. Theta and phi are the far-field angles Θ and Φ from Fig. 1. The first side lobes are

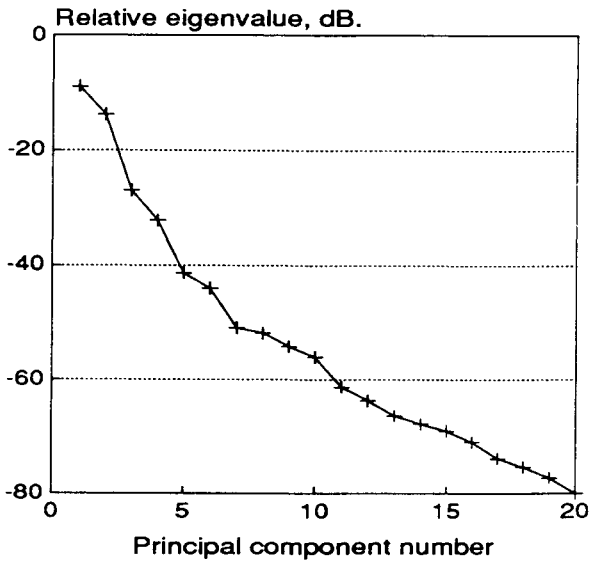

Fig. 6 Principal component eigenvalues.

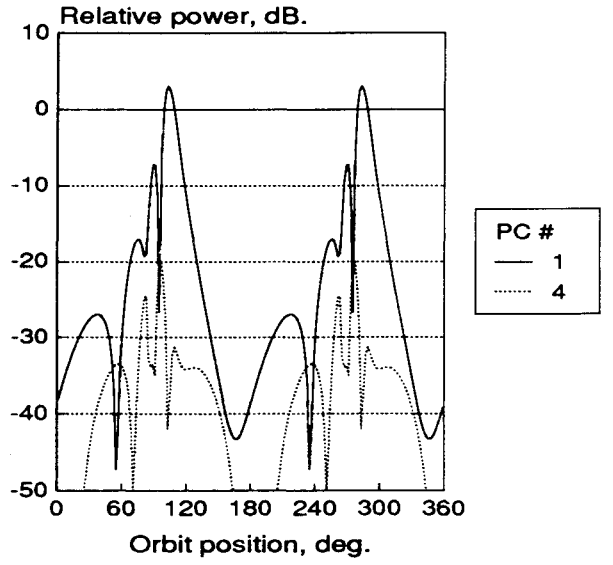

Fig. 7 Variation of power for first and fourth PCs.

seen to be at the -30 dB level. The difference between the sections could be reduced by selecting a smaller spacing for the numerical integration, but the 1-dB difference in the first side lobe is accurate enough for the purposes here.

Control with Perfect Knowledge

This section will discuss the design and performance of a control system assuming that there is perfect knowledge of the system and its environment. The system will be designed with the nominal conditions being the Sun at equinox and the shadow of the Earth neglected. At orbit position zero, the Earth and Sun are at opposition as seen from the spacecraft. With these assumptions, the design proceeded by mapping the thermal distortions into the radio frequency (RF) parameters, by performing a principal component analysis, by determining optimal actuator locations, and finally by determining the optimal actuator strokes.

1. Mapping Thermal Distortion into RF Parameters

The $G(t)$ matrices of Eq. (11) were calculated at 180 equally spaced orbital positions. During this process, the value of J_1 of Eq. (17) was determined to identify the orbital position (Fig. 4) where the far field will be most distorted. A double extrema in J_1, referenced to A_{00}^2, occurs when the Sun is illuminating the edge of the antenna, which is the position of maximum temperature differences between structural rods. The corresponding far-field pattern (Fig. 5) is unacceptable when compared to Fig. 3 because of the central beam broadening and the increase in side lobe levels. Note that, for 50% of the orbit, the value of J_1 exceeds -20 dB. It will be seen later that this is about the maximum value of J_1 that will meet the -28 dB side lobe goal.

2. Principal Component (PC) Analysis

The Grammian H of Eq. (12) is approximated by averaging the 180 GG^T matrices from which the 20 largest eigenvalues of H and corresponding eigenvectors were extracted. The eigenvalue results are shown in Fig. 6, and the variation of the power, $g_i^T g_i$ from Eq. (16), for the first and fourth PCs is shown in Fig. 7. Each PC is expected to contribute its maximum distortion to the far field at the time of maximum amplitude. The first PC with maximum J_1 cost of $+3$ dB must clearly be controlled, and the fourth, with a maximum J_1 of -19.9 dB, is a borderline case at -28 dB (Fig. 8). The fifth and higher PC can be neglected except for any spillover effects. From these and other[7] results, a criterion of -20 dB is selected as the maximum value of J_1 that is acceptable. That is, acceptable performance can be maintained as long as the dis-

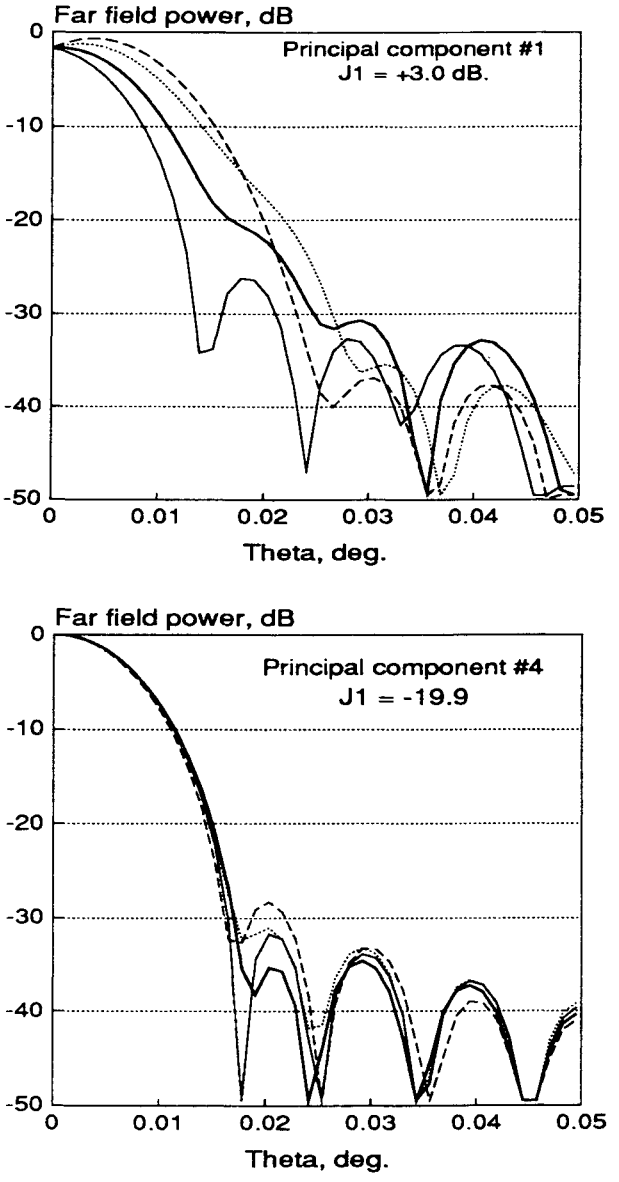

Fig. 8 Far-field pattern for first and fourth PCs at maximum power.

tortion part of the far field contributes no more than 1% of the peak power.

3. Optimal Actuator Locations

Initially, all 420 rods in the structure (Fig. 2) were considered as potential sites for the actuators. To perform the initial screening using Eq. (28) requires an assumption of the number L of PCs to be included in determining the effectiveness ϵ_α. Step 2 earlier suggests that L must be 4 or greater. Selecting L to be 4 would assure control under the nominal conditions but may not provide a robust system that can accommodate off-nominal conditions that no doubt will "excite" higher PCs. On the other hand, picking L too large assures that higher PCs will be "excited" while controlling only the lower PCs. Two values of L (5 and 10) were selected for testing, and for both cases it was found that the 156 front surface rods (Fig. 9) produced larger average values of ϵ_α than did either back surface rods or intermediate rods,[7] and no further consideration was given to back and middle rods. A pairwise comparison was made using Eq. (29), and the least effective location of any pair with $\epsilon_{\alpha\beta} > 0.99$ was removed from consideration, leaving 65 and 82 candidate sites when $L = 5$ and 10, respectively.

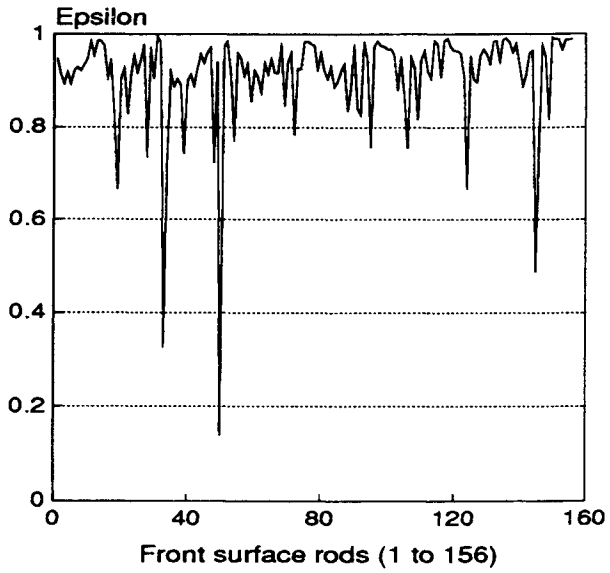

Fig. 9 Rod effectiveness ratio ϵ_α for $L = 5$.

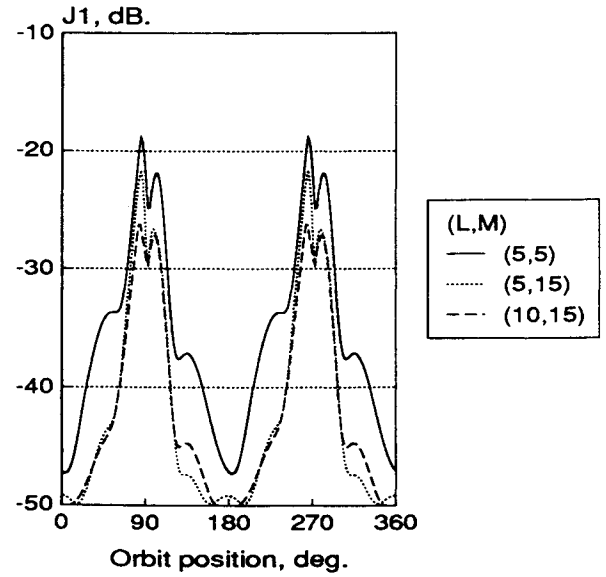

Fig. 10 Effect of varying L and M on nominal condition cost.

Having identified the potential locations, a "two steps forward/one step back" approach was used to select the actuator locations. In this approach, Eqs. (26) and (27) are used sequentially to add two actuator locations to the selected set, then the actuator that has been in the selected set the longest is deleted. Each cycle of this process only adds one actuator. This procedure provided some confidence in the final results because it was found that after only a few cycles the deleted location was generally immediately returned to the set. Though suboptimal, the process is adequate for the purpose here and is computationally efficient. Suboptimal locations[7] were generated with 5 and 10 principal components ($L = 5,10$) of Eq. (28) and with varying number of actuators ($5 \le M \le 20$) of Eq. (20).

4. Optimal Actuator Strokes

Given a set of actuator locations, the optimal stroke variations of Eq. (21) and J_1 of Eq. (24) can be calculated throughout the orbit. Actuator strokes were generally less than 1 mm.[7] Figure 10 shows the variation of J_1 for three cases. It was generally found that the best performance is achieved when M is slightly larger than L. Though not shown, the first side lobe is at -29.2 dB for $L = M = 5$; thus, as few as five actuators can control the far-field pattern to acceptable levels under nominal conditions. Off-nominal cases, described next, demonstrated the inability of this system to meet the performance goals.[7]

Control with Estimated Knowledge and Off-Nominal Conditions

In this case, measurements of surface deviations at one time are used to estimate one column of the G matrix using Eqs. (31) and (32), from which the full $\hat{G}$ matrix at the same time can be formed. Then the actuator strokes will be calculated from Eq. (21) with $\hat{G}$ replacing G on the right side. No attempt to optimally locate sensors was performed; rather, two arrays of sensors were assumed as shown in Fig. 11. Thirteen sensors are denoted by circles at the nodes to which the sensor is assumed to be attached. In the second case, an additional 6 sensors, denoted by the squares, are on the perimeter to give a total of 19. These two cases will be denoted by $S = 13$ and 19, respectively. The next issue is how many principal component amplitudes to estimate using Eq. (31). Two values were selected for this study, $P = 5$ and 10, respectively.

A performance simulation is characterized by four integers: L, the number of principal components used to determine rod effectiveness, Eq. (28); M, the number of actuators, Eq. (20); P, the number of PC amplitudes estimated from the measurements, Eq. (30); and S, the number of sensors, Eq. (30). In what follows, the system will be denoted by (L,M,P,S).

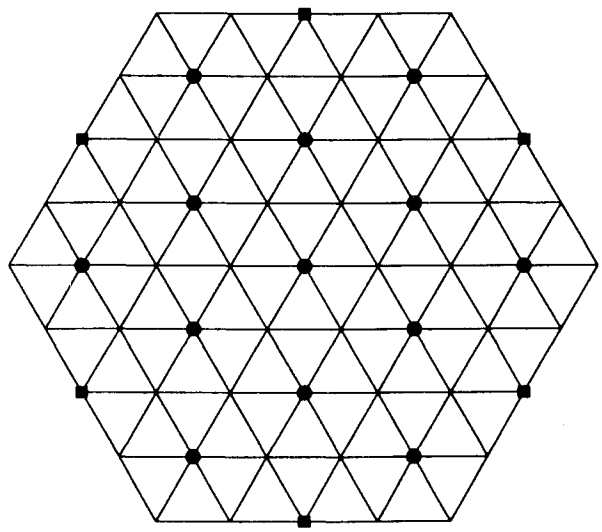

Fig. 11 Sensor locations on front surface nodes.

1. Effects of Deviations from the Orbital Conditions

The nominal conditions ignored the shadow of the Earth and assumed the Sun to be in the equatorial plane. Including the shadow produced no difficulty for the minimal system (5,5,5,13)[7] because when the antenna is in the shadow, it is nearly isothermal, and shadow effects disappear in a few minutes after exiting. When the Sun is at 23.5° latitude, the minimal system is not adequate because of asymmetrical heating and the number of actuators must be increased to at least 11.[7] For $L = 5$ and $M = 11$, Fig. 12 shows the influence of changing S and P on the closed-loop performance. Calculation of the far-field at maximum J_1 demonstrates that the system (5,11,10,13) meets the -28 dB side lobe goal.

2. Effects of System Errors

The control system must also be able to accommodate system errors. For example, individual elements of the structure will vary in cross-section measurements, in elastic modulus, in coefficient of thermal expansion, emissivity, absorbtivity, etc. To quantify the effectiveness of the control system, a number of simulations were performed. In the first simulation, the 420 rods in the structure were assumed to have errors in tensile stiffness that are uniformly distributed between $\pm 2\%$.[16] For this simulation one random sample showed that the (5,5,5,13) system returned the cost to within 1 dB of the nominal case.

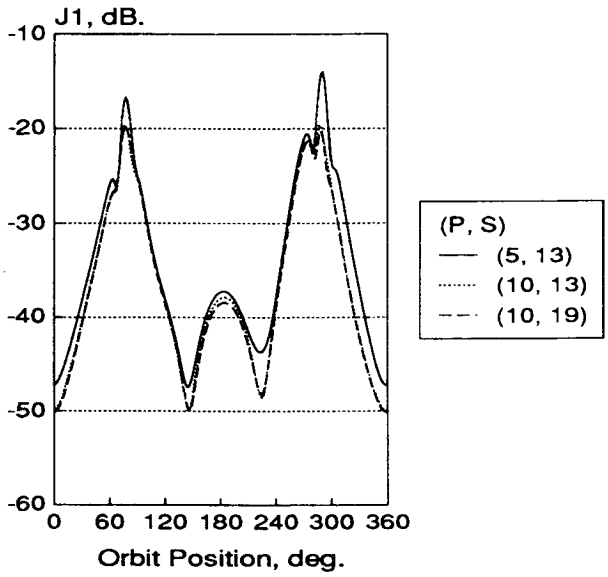

Fig. 12 Cost for Sun at 23.5° declination.

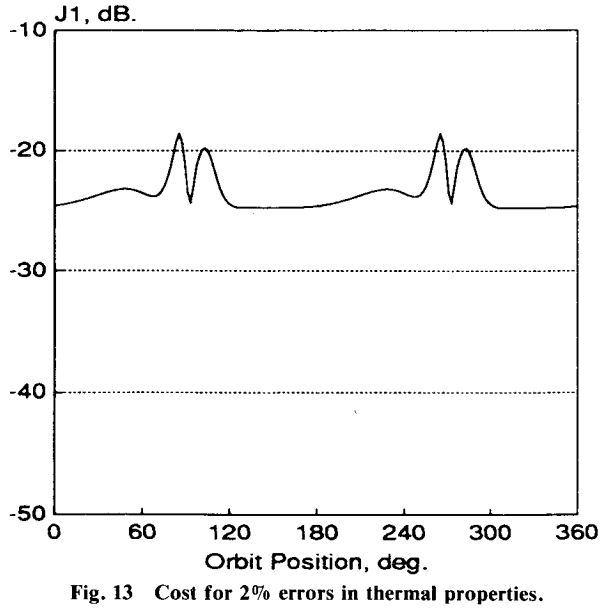

Fig. 13 Cost for 2% errors in thermal properties.

Second, errors in the thermal properties of the structure were considered, specifically, the coefficient of thermal expansion (CTE), the emissivity ϵ, and the absorptivity α. These parameters directly determine the temperature of the rods and/or directly influence the surface distortion. The error in CTE due to manufacturing process would be due to the same type of errors that produce variations in stiffness; thus, a 2% uniform distribution is assumed for CTE. Optical properties for coating can vary greatly during the manufacturing process and can change with age in orbit. However, the rods for GEO can be uncoated graphite epoxy and nearly black. Thus, only small variations in α and ϵ are expected. Again a uniform distribution of 2% is selected. The control system (5,5,5,13) produced a maximum value for J_1 of -18.5 dB; however, the variation of cost throughout the orbit is significantly different as seen in Fig. 13. Whereas for previous simulations the cost decreased significantly away from the peak, this is not true for this case. The reason for this behavior is that 2% variations in the emissivity and absorptivity produce random variations in the aperture phase. These random variations produce a background in J_1 of about -24 dB that cannot be corrected by so few actuators. The far zone field does, however, meet the -28 dB goal.

VII. Concluding Remarks

A theoretical basis has been developed for controlling the distortions of large space, Earth-pointing radiometers due to thermal variations during orbital motion. A control system cost function that is quadratic in form and is directly related to radiometer performance has been developed by expanding the far zone electric field in a Zernike-Bessel series. In this expansion a quadratic cost function naturally appears, and it is found that this cost is a consistent indicator of the deviation of the far field from the desired pattern. The temporal variations have been included in the development of the optimal actuator locations by expanding the aperture integral using a principal component analysis. It is shown that the eigenvalues are directly related to average deviations of the far-field pattern from the desired pattern. Further, the eigenvectors are used as a basis for directly estimating far-field deviations from sensors measurements. The approach provides a rationale for determining the minimum number of actuators and sensors.

Simulations for a geosynchronous radiometer demonstrated the need for the closed-loop system and demonstrated that the method provides a convenient means to design an effective control system, some physical insight into the design process, and a convenient means to quantify the influence of various orbit geometries and deviations of the system due to manufacturing and other errors.

References

[1]Padula, S. L., Adelman, H. M., Bailey, M. C., and Haftka, R. T., "Integrated Structural Electromagnetic Shape Control of Large Space Antenna Reflectors," *AIAA Journal,* Vol. 27, No. 6, 1989, pp. 814–819.

[2]Haftka, R. T., and Adelman, H. M., "Selection of Actuator Locations for Static Shape Control of Large Space Structures by Heuristic Integer Programming," *Computers and Structures,* Vol. 20, Nos. 1-3, 1985, pp. 575–582.

[3]Chen, G. S., Garba, J. A., Wada, B. K., "Vibration Suppression for the Precision Segmented Reflector Backup Structure," *Proceedings of Active Telescope Systems Meeting,* Society of Photo-Optical Instrumentation Engineers, 1989, pp. 508–520.

[4]Hardy, J. H., "Active Optics—Don't Build a Telescope Without It!," *Proceedings of International Conference on Advanced Technology Optical Telescopes,* Society of Photo-Optical Instrumentation Engineers, Vol. 332, March 1982, pp. 252–259.

[5]Haftka, R. T., and Adelman, H. M., "An Analytical Investigation of Shape Control of Large Space Structures by Applied Temperature," *AIAA Journal,* Vol. 23, No. 3, 1985, pp. 450–457.

[6]Collin, R. E., and Zucker, F. J., *Antenna Theory,* Pts. 1 and 2,

McGraw-Hill, New York, 1969.

[7]Tolson, R. H., "Integrated Control of Thermally Distorted Large Space Antennas," Ph.D. Dissertaiton, Old Dominion Univ., Norfolk, VA, Dec. 1990.

[8]Balanis, C. A., *Antenna Theory, Analysis and Design,* Harper & Row, New York, 1982.

[9]Mattra, R., Rahmat-Samii, Y., Galindo-Israel, V., and Norman, R., "An Efficient Technique for the Computation of Vector Secondary Patterns of Offset Paraboloid Reflectors," *IEEE Transactions on Antennas and Propagation,* Vol. AP-27, No. 3, 1979, pp. 294–304.

[10]Born, M., and Wolf, E., *Principles of Optics,* Pergamon Press, New York, 1987.

[11]Noll, R. J., "Zernike Polynomials and Atmospheric Turbulence," *Journal of the Optical Society of America,* Vol. 66, No. 3, 1976, pp. 207–211.

[12]Moore, B. C., "Principal Component Analysis in Linear Systems: Controllability, Observability, and Model Reduction," *IEEE Transactions on Automatic Control,* Vol. AC-26, No. 1, 1981, pp. 17–32.

[13]Kubrusly, C. S., and Malebrache, H., "Sensor and Controller Locations in Distributed Systems—A Survey," *Automatica,* Vol. 21, No. 2, 1985, pp. 117–128.

[14]Garrett, L. B., "Interactive Design and Analysis of Future Large Spacecraft Concepts," NASA TP 1937, Dec. 1981.

[15]Mahaney, J., and Strode, K. B., "Fundamental Studies of Thermal-Structural Effects on Orbiting Trusses," *Proceedings of the AIAA 23rd Structures, Structural Dynamics and Materials Conference,* Pt. 1, AIAA, New York, 1982, pp. 49–59; CP 823.

[16]Bush, H., private communication, Langley Research Center, 1990.